JOURNAL OF SOLID STATE CHEMISTRY 109, 259–264 (1994)

Hydrothermal Synthesis, Crystal Structure, and Magnetic Properties of $Cs[(V_2O_3)(HPO_4)_2(H_2O)]$, a Mixed-Valence Vanadium (IV, V) Hydrogen Phosphate with a One-Dimensional ($-V^{IV}-O-V^{V}-O-$) Chain of Corner-Sharing VO_6 Octahedra

Robert C. Haushalter,* Zhanwen Wang,†,‡,[1] Mark E. Thompson,‡ Jon Zubieta,† and Charles J. O'Connor§

*NEC Research Institute, 4 Independence Way, Princeton, New Jersey 08540; †Department of Chemistry, Syracuse University, Syracuse, New York 13244; ‡Department of Chemistry, Princeton University, Princeton, New Jersey 08544; and §Department of Chemistry, University of New Orleans, New Orleans, Louisiana 70148

Received August 26, 1992; in revised form July 19, 1993; accepted July 22, 1993

The hydrothermal reaction of $Cs_4V_2O_7$, V, H_3PO_4, H_2O, and Bu_4NBr in the molar ratio 4.5:1:41:3150:1 at 200°C for 48 hr yielded the red-brown cesium vanadium phosphate $Cs[(V_2O_3)(HPO_4)_2(H_2O)]$, a mixed-valence V(IV, V) species. The structure contains corner-sharing vanadium octahedra and phosphorus tetrahedra with unusual 1-D $(-V^{IV}-O-V^{V}-O-)\infty$ chains formed from VO_6 octahedra sharing opposite corners. These chains are connected through tridentate bridging $(HPO_4)^{2-}$ units to produce a three-dimensional network. The Cs^+ cations occupy large channels formed from six vanadium octahedra and six phosphorus tetrahedra. At room temperature the material is paramagnetic with one unpaired spin per $(-V^{IV}-O-V^{V}-O-)$ unit while complicated antiferromagnetic ordering is observed below ca. 6 K. Crystal data: monoclinic, $P2_1/n$ with $a = 7.22(1)$, $b = 18.56(1)$, $c = 8.195(6)$ Å, $\beta = 114.01(6)°$, $Z = 4$, $d_{calc} = 3.233$ g cm^{-3}; structure solution and refinement based on 1088 reflections converged at $R = 0.028$.

INTRODUCTION

The extensive contemporary interest in the vanadium phosphate system reflects the catalytic relevance (1) of the oxovanadium(V) phases (2–5) and the variety of low-dimensional magnetic interactions exhibited by reduced phases (6–12). Furthermore, the introduction of other cations to produce compositions of the $M^{n+}-V^{m+}-P-O$ system allows a dramatic expansion of the structural chemistry of these phases, giving a variety of lamellar and channel structures with the cations located in the interlamellar regions or occupying the hydrophilic channels (13–27). While these extended structures may be described in gross terms as networks of corner-sharing vanadium octahedra and phosphorus tetrahedra, the detailed connectivities achieved by these simple geometric types exhibit dramatic flexibility, producing a rich and varied structural chemistry. The structural types adopted by these phases reflect not only the identity of the cation M^{n+} but also the vanadium oxidation state, the pH of the solution and consequently the degree of protonation of the phosphate residues $(H_nPO_4)^{(3-n)-}$ ($n = 0$, 1, or 2), as well as the presence of aquo coligands. In an effort to gain some insight into synthesis-structure relationships, we have begun a study of the hydrothermal synthesis of alkali metal phases of reduced vanadium phosphates (28–29). As part of these investigations, we have prepared a novel mixed-valence V(IV, V) species $Cs[(V_2O_3)(HPO_4)_2(H_2O)]$ **(1)** whose structure contains $(-V^{IV}-O-V^{V}-O-)\infty$ chains linked so as to form a three-dimensional network with cation encapsulating channels. The magnetic properties of the vanadium centers were also studied.

EXPERIMENTAL

Synthesis. The hydrothermal reaction of $Cs_4V_2O_7$, V(−325 mesh), H_3PO_4, H_2O, and Bu_4NBr in the molar ratio 4.5:1:41:3150:1 at 200°C for 48 hr gave a two-phase mixture of **(1)** and an unidentified material in a ratio of ca. 2:1. Several variations of the reaction conditions were carried out but it was not possible to produce single-phase **(1)** free of the impurity.

Crystallography. The experimental crystallographic data are collected in Table 1, the atomic coordinates and isotropic temperature factors are in Table 2, and some selected bond distances are in Table 3.

Magnetic measurements. The magnetic susceptibility data were recorded on a manually selected, 115-mg poly-

[1] On leave from Nanjing Institute of Technology.

0022-4596/94 $6.00

TABLE 1
Experimental Crystallographic Details

A. Crystal data	
Empirical formula	$CsV_2P_2O_{12}H_4$
Crystal color, habit	red-brown, prism
Crystal dimensions (mm)	0.30 × 0.30 × 0.20
Crystal system	Monoclinic
Lattice parameters:	a = 7.22 (1) Å
	b = 18.56 (1) Å
	c = 8.195 (6) Å
	β = 114.01 (6) °
	V = 1004 (1) Å^3
Space group	$P2_1/n$ (#14)
Z value	4
D_{calc}	3.233 g/cm^3
μ(Mo$K\alpha$)	57.24 cm^{-1}
B. Intensity measurements	
Diffractometer	Rigaku AFC6S
Radiation	Mo$K\alpha$(λ = 0.71069 Å)
Temperature	23°C
$2\theta_{max}$	45.0°
No. of reflections measured	Total: 1485
Corrections	Lorentz-polarization
	absorption
	(trans. factors: 0.83–1.19)
	Secondary extinction
	(coefficient: 0.17050 × 10^{-6})
C. Structure solution and refinement	
Structure solution	Direct methods
Refinement	Full-matrix least-squares
Function minimized	$\Sigma\, w(\|F^o\| - \|F_c\|)^2$
Least-squares weights	$4F_o^2/\sigma^2(F_o^2)$
p-factor	0.01
Anomalous dispersion	All non-hydrogen atoms
No. of observations ($I > 32.00\ \sigma(I)$)	1088
No. of variables	155
Reflection/parameter ratio	7.02
Residuals: R; R_w	0.028; 0.034
Goodness of fit indicator	2.98
Maximum peak in final diffraction map	0.63 e$^-$/Å^3
Minimum peak in final diffraction map	−0.61 e$^-$/Å^3

crystalline sample of $Cs[V_2O_3(HPO_4)_2H_2O)]$ over the 2–300 K temperature range using a Quantum Design MPMS SQUID susceptometer. Measurement and calibration techniques have been reported elsewhere (31).

RESULTS AND DISCUSSION

Red-brown crystals of $Cs[(V_2O_3)(HPO_4)_2H_2O)]$ (**1**) were obtained from the hydrothermal treatment of $Cs_4V_2O_7$, V(−325 mesh), H_3PO_4, H_2O, and Bu_4NBr in the molar ratio 4.5 : 1 : 41 : 3150 : 1 at 200°C for 48 hr. The presence of a reducing agent, in this case V metal, is necessary to reduce the V^{5+} starting materials and to avoid formation of phases of the $M_{0.50}VOPO_4 \cdot nH_2O$ class (M = alkali metal) (20) and Keggin ion related materials. On the other hand, the presence of a greater excess of V metal can lead to the V(III) phosphate phase $Cs[V_2(PO_4)(HPO_4)_2H_2O)_2]$ (29).

TABLE 2
Positional Parameter and B_{eq} for $Cs[V_2O_3(HPO_4)_2H_2O)]$

Atom	x	y	z	B(eq)
Cs(1)	0.14524(9)	0.13212(3)	0.51750(7)	2.60(3)
V(1)	0.1714(2)	0.12363(7)	1.0210(2)	0.88(5)
V(2)	−0.3308(2)	0.14162(7)	1.0185(2)	1.19(5)
P(1)	0.2290(3)	−0.0262(1)	1.2332(3)	0.98(8)
P(2)	0.0226(3)	0.2785(1)	0.8076(3)	0.98(8)
O(1)	0.3005(7)	0.2029(3)	1.1941(6)	1.1(2)
O(2)	0.0490(7)	0.1975(3)	0.8273(7)	1.2(2)
O(3)	0.3685(7)	0.1065(3)	0.9767(6)	1.3(2)
O(4)	−0.0797(7)	0.1462(3)	1.0835(7)	1.3(2)
O(5)	−0.0080(7)	0.0499(3)	0.8581(6)	1.1(2)
O(6)	0.2473(7)	0.0554(3)	1.2265(6)	1.2(2)
O(7)	−0.4207(8)	0.2068(3)	0.8794(7)	2.1(2)
O(8)	−0.3672(7)	0.0649(3)	0.8377(7)	1.4(2)
O(9)	−0.2712(8)	0.0408(3)	1.2042(7)	1.8(2)
O(10)	−0.3363(7)	0.1860(3)	1.2336(7)	1.9(2)
O(11)	0.3028(8)	−0.0435(3)	1.4388(7)	1.7(2)
O(12)	0.0765(7)	0.3128(3)	1.0001(6)	1.5(2)

Note. $B_{eq} = \frac{8\pi^2}{3}[U_{11}(aa^*) + U_{22}(bb^*) + U_{33}(cc^*) + 2U_{12}aa^*bb^*\cos\alpha + 2U_{13}aa^*cc^*\cos\beta + 2U_{23}bb^*cc^*\cos\alpha]$.

TABLE 3
Intramolecular Distances in (1)

Atom	Atom	Distance
V(1)	O(1)	1.993(5)
V(1)	O(2)	2.010(5)
V(1)	O(3)	1.638(5)
V(1)	O(4)	2.118(5)
V(1)	O(5)	1.981(5)
V(1)	O(6)	1.998(5)
V(2)	O(3)	2.158(6)
V(2)	O(4)	1.673(5)
V(2)	O(7)	1.608(6)
V(2)	O(8)	1.994(5)
V(2)	O(9)	2.339(5)
V(2)	O(10)	1.961(5)
P(1)	O(5)	1.527(5)
P(1)	O(6)	1.523(5)
P(1)	O(8)	1.524(5)
P(1)	O(11)	1.580(6)
P(2)	O(1)	1.531(5)
P(2)	O(2)	1.516(5)
P(2)	O(10)	1.531(5)
P(2)	O(12)	1.595(5)

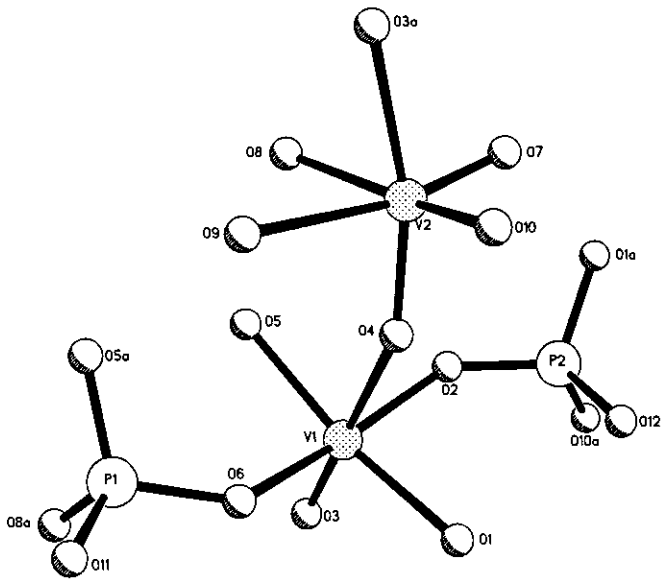

FIG. 1. The primary building block of the structure of $Cs[(V_2O_3)(HPO_4)_2H_2O)]$, (1), showing the atom-labeling scheme. The aquo ligand is O9.

The structure of **1** consists in gross geometry of a network of corner-sharing vanadium octahedra and phosphorus tetrahedra. Figure 1 illustrates the primary building blocks of the structure. The crystallographically and chemically unique vanadium sites display distorted octahedral geometry. The V1 center exhibits corner-sharing interactions with oxygen atoms from four phosphorus tetrahedra and connectivity to adjacent V2 sites through a pair of shared *trans* oxo-groups (30). The oxo-groups assume nonsymmetrical bridging modes, such that the V1–O3 and V1–O4 distances are 1.638(5) and 2.118(5) Å, respectively. The V2 center coordinates to two oxygens of two corner-sharing phosphorus tetrahedra, the oxygen donor of an aquo ligand, a terminal oxo-group *trans* to this a quo ligand, and the *trans* oxo-groups which serve to form the chain of corner-sharing vanadium octahedra. This chain of fused octahedra provides the structural motif shown in Fig. 2a by expansion of the basic unit of Fig. 1 along the crystallographic **a** direction. A 1-D chain of corner-sharing octahedra was also found in some $MVPO_5$ materials (18) but usually with all of the V atoms crystallographically identical and in the 4+ oxidation state.

Several features of the chain geometry are noteworthy. The V–O–V bridges are distinctly nonsymmetrical as noted above. There is thus a short–long–short–long repeat along the O3–V1–O4–V2–O3*a* chain which localizes the multiple bond character in the V1–O3 and V2–O4 interactions. Such nonsymmetrical V–O–V bonding has been observed previously in the structures of polyoxovanadates, such as $[V_{10}O_{28}]^{6-}$ (32), $[H_2V_{10}O_{28}]^{4-}$ (32) and $[H_3V_{10}O_{28}]^{3-}$ (34), as well as in $NaVOPO_4$ (18). The V2 center exhibits a *cis* dioxo unit (VO_2), with one oxo-group displaying a conventional terminal and multiply bonded geometry and the second involved in the nonsymmetrical bridge. Valence sum calculations (34) clearly identify V2 as a V^{5+} site, while V1 is the V^{4+} site. The clearly distinguishable geometries associated with V1 and V2 thus identify **1** as a Class I mixed-valence system with spin localization on the V1–d^1 center (36). The corner-shared vanadium chains may be thus described as $(-V^{IV} = O-V^{V} = O-)_\infty$ strings. The magnetic properties of the d^1 center are discussed below.

As shown in Fig. 2b, pairs of corner-sharing vanadium octahedra in the chain are bridged in a bidentate fashion by $(HPO_4)^{2-}$ tetrahedra. Moreover, adjacent chains of vanadium octahedra are linked through $(HPO_4)^{2-}$ tetrahedra. Morevoer, adjacent chains of vanadium octahedra are linked through $(HPO_4)^{2-}$ tetrahedra to produce the three-dimensional network characteristic of the structure of **1**. Also shown in Fig. 2b, which is a projection of the unit-cell contents parallel to the chain direction (down[100]), are the infinite chains which are isolated from one another by $\{HPO_4\}$ groups. This view also shows the manner in which the $\{HPO_4\}$ groups line the tunnels that run parallel to [100].

The view of the packing along the crystallographic **a** axis, shown in Fig. 2b, reveals the channels that are formed by the corner sharing of octahedra and tetrahedra. As depicted in Fig. 3, the Cs^+ cations occupy these hydrophilic tunnels, into which the pendant –OH groups of the $(HPO_4)^{2-}$ groups also project. It is instructive to compare the structure of the cation channel in **1** with that of β-$RbV(HPO_4)_2$ (28). Both structures provide cation channels formed from edge sharing of six vanadium octahedra and six phosphorus tetrahedra with four pendant –OH groups projecting into the channel. Furthermore, adjacent channels are linked through a four connect domain of two vanadium octahedra and two phosphorus tetrahedra. Even though the two types of tunnel are constructed of the same number and types of polyhedra, the tunnels of β-$RbV(HPO_4)_2$ are puckered and collapsed about the relatively smaller Rb^+ as compared to the tunnels in (**1**) that are formed about the larger Cs^+.

Magnetic susceptibility measurements on (**1**) (Fig. 4) reveal complicated antiferromagnetic behavior at low temperatures. The high-temperature magnetic susceptibility data ($T > 50$ K) exhibit Curie–Weiss paramagnetism, $\chi = C/(T - \theta)$, with $C = 0.316$ emu-K/mole and $\theta = -9.8$ K. The electron structure of $CsV_2O_3(HPO_4)_2(H_2O)$ corresponds to one unpaired electron per V_2O_3 formula unit. This results in a Curie–Weiss g value of $g = 1.83$ for the V(IV) centers.

At lower temperatures an anomaly is observed in the temperature dependence of the magnetic susceptibility.

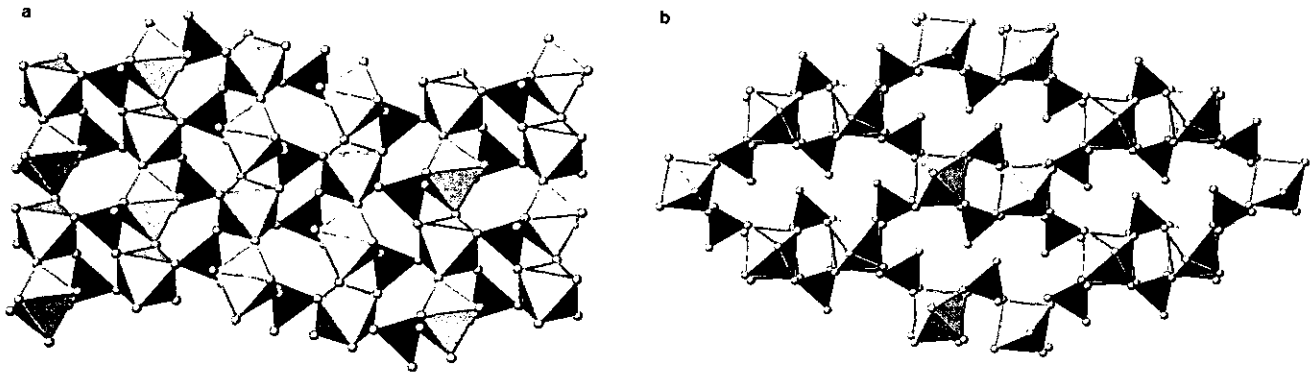

FIG. 2. (a) View of the structure of (1) perpendicular to the 1-D chains (parallel to **c** with **a** vertical and **b** horizontal), showing the infinite chains of corner-linked vanadium octahedra. (b) Expansion of the structural motif viewed down **a**, showing the linkage of parallel chains.

As the temperature is lowered to around 5 K, the magnetic susceptibility of the sample passes through a maximum and begins to decrease. This behavior is often associated with short-range antiferromagnetic exchange in a crystal lattice. Structurally, there are two features that might influence the magnetic properties. First, the material is a structural linear chain that is propagated along the –V(IV)–O–V(V)–O–V(IV)– bonding pathway. Another structural feature is the presence of a doubly bridged V(IV)–(O–P–O–)2–V(IV) binuclear units in the unit cell. The binuclear $V(IV)_2$ units are interconnected by several other single phosphate bridges to other pairs of V(IV) to form sheets. The observed magnetism most likely has contributions from both of these sources.

We attempted to approximate the magnetic interactions with both a one dimensional and a dimer model. If the one dimensional model were operative, the magnetic exchange that would be expected in the d^1 vanadium(IV) with spin $S = 1/2$ is the isotropic Heisenberg spin Hamiltonian ($H = 2JS_2 \cdot S_2$). The behavior of a one-dimensional Heisenberg linear chain has been described by Bonner and Fisher (37). The Bonner–Fisher Heisenberg linear chain model was applied to the data to determine if the short-range order arises from the one-dimensional magnetic interaction. The high-temperature data in the Curie–Weiss region could be fit adequately with this model; however, the Bonner–Fisher model did not satisfactorily fit the region of the maximum.

Since there is a potential cross exchange through the phosphate bridges, a molecular field correction to the linear chain model was used to approximate the effect of interchain interactions. The equation that describes the effect of a molecular exchange field is

$$\chi = \frac{\chi'}{1 - (zJ'/Ng^2\mu^2)\chi'} + \text{TIP}, \qquad [1]$$

where χ' is the magnetic susceptibility of the linear chains in the absence of the exchange field and χ is the molecular exchange field influenced magnetic susceptibility that is

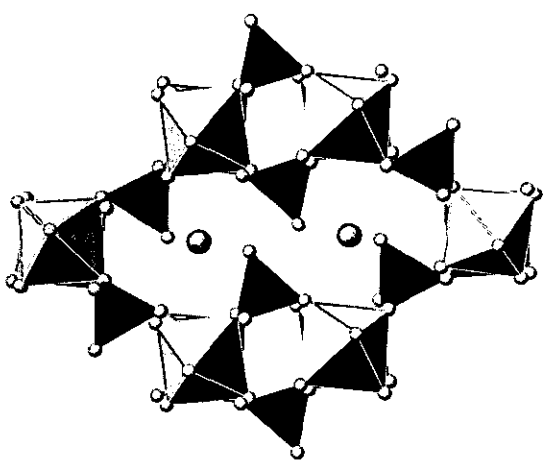

FIG. 3. A polyhedral representation of the structure of (1) parallel to **a** showing the hydrophilic, $\{HPO_4\}$-lined tunnels, and Cs^+ cations.

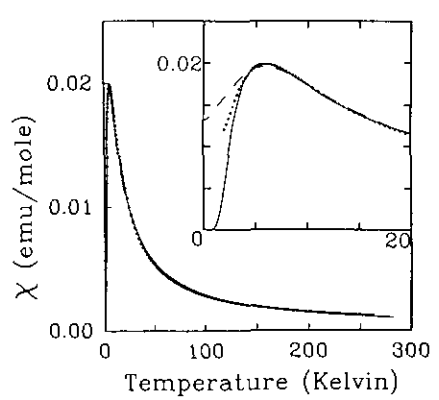

FIG. 4. The magnetic susceptibility of (1) as a function of temperature. The inset is an expansion of the low temperature region (see text).

actually measured. The exchange field coupling parameter is zJ', where z is the number of exchange-coupled neighbors. The addition of the molecular field exchange correction improved the fit to the data only slightly.

A greater improvement of the fit to the data could be obtained by neglecting the data at temperatures below 3.5 K. The results of this fit of the Bonner–Fisher model to the magnetic data is illustrated as the dashed curve in the inset of Fig. 4 The parameters used in the fit were $g = 1.72$, $JZ/k = -4.6$ K, and $zJ'/k = 2.3$ K. In addition, a temperature-independent paramagnetism term (TIP) of 0.00013 emu/mole was required. However, the fact that the model does not reproduce all the observed features at the lower temperatures indicates that other exchange mechanisms must also be operative.

Since the magnetic suspectibility data appear to drop below the Bonner–Fisher model at the lowest temperatures, a fit of the data to the dimer model was attempted. The magnetic susceptibility equation that describes the behavior expected for a binuclear $S_1 = S_2 = 1/2$ system is given in Eq. [2] where $x = J/kT$ and $2J$ is the separation of the singlet and triplet states, with a negative J denoting a ground singlet.

$$\chi = \frac{2Ng^2\mu^2}{kT}\left(\frac{e^{2x}}{1+3e^{2x}}\right). \qquad [2]$$

Following the same procedure used for the linear chain analysis, we fit Eq. [2], corrected for interbinuclear exchange with the molecular field approximation (eq. [1]). The results of the fit of the magnetic data to Eq. [2] corrected for interdimer interactions with Eq. [1], is illustrated in Fig. 4 as the smooth line drawn through the data. The fitted parameters are $g = 1.80$, $J/k = -4.6$ K and $zJ'/k = -7.5$ K. In addition, a temperature-independent paramagnetism term of TIP = 0.00003 emu/mole was required. The fact that the correction term zJ'/k in this model is larger than J/k indicates that the lower temperature behavior has not been fully modeled.

The dimer model gives a better fit over the temperature range 3.5–200 K. Neither model can satisfactorily fit the data below 3.5 K. Recent reports of vanadium phosphate clusters have shown that the V(IV) ions show a propensity for dimer formation within the solid framework, and the magnetic data for these materials has been successfully treated with the interacting dimer mode (10, 12). The value of zJ' is rather large for $CsV_2O_3(HPO_4)_2(H_2O)$ and therefore should be viewed only as an indication of strong interbinuclear coupling, and not as a quantitative estimate of that coupling. However, the primary exchange constant ($J/k = -4.6$ K for both models) does give an indication of the strength of the magnetic interactions in this material.

ACKNOWLEDGMENT

The work at Syracuse University was supported by NSF Grant CHE 9119910.

REFERENCES

1. O. Centi, F. Trifiro, J. R. Ebnar, and V. M. Franchetti, *Chem. Rev.* **88,** 55 (1988).
2. G. Z. Ladwig, *Anorg. Allg. Chem.* **338,** 266 (1965); E. Bordes, and P. Courtine, *C.R. Seances Acad. Sci., Ser. C.* **274,** 1375 (1972).
3. M. Tachez, F. Theobald, and E. Bordes, *J. Solid State Chem.* **40,** 280 (1981); B. D. Jordan and C. Calvo, *Acta Crystallogr., Sec. B* **32,** 2899 (1976).
4. E. Bordes, P. Courtine, and G. Pannetier, *Ann. Chim. (Rome)* **8,** 105 (1973).
5. D. Ballutand, E. Bordes, and P. Courtine, *Mater. Res. Bull.* **17,** 519 (1982); M. Tachez, F. Theobald, J. Bernard, and A. W. Hewat, *Rev. Chim. Miner.* **19,** 291 (1982).
6. A. LeBail, G. Ferey, P. Amoros, and D. Beltran-Porter, *Eur. J. Solid State Inorg. Chem.* **26,** 419, (1989).
7. A. LeBail, G. Ferey, P. Amoros, D. Beltran-Porter, and G. Villeneuve, *J. Solid State Chem.* **79,** 169 (1989).
8. C. C. Torradi and J. C. Calabrese, *Inorg. Chem.* **23,** 1308 (1984).
9. M. E. Leonowitz, J. W. Johnson, J. F. Brody, and H. F. Shannon, *J. Solid State Chem.* **56,** 370 (1985).
10. E. Bordes and P. Courtine, *J. Chem. Soc., Chem. Commun.*, 294 (1985); D. C. Johnston, J. W. Johnson, D. P. Goshorn, and A. J. Jacobson, *Phys. Rev. B* **35,** 219 (1987).
11. G. Ladwig, *Z. Chem.* **19,** 386 (1979).
12. J. W. Johnson, D. C. Johnston, H. E. King, Jr., T. R. Halbert, J. F. Brody, and D. P. Goshorn, *Inorg. Chem.* **27,** 1646 (1988).
13. K. H. Lii, and H. J. Tasi, *J. Solid State Chem.* **90,** 291 (1991).
14. K. H. Kii, Y. P. Wang, S. L. Wang, *J. Solid State Chem.* **80,** 127 (1989).
15. K. H. Lii, H. J. Tsai, and S. L. Wang, *J. Solid State Chem.* **87,** 396 (1990).
16. K. H. Kii and S. L. Wang, *J. Solid State Chem.* **82,** 239 (1989).
17. K. H. Lii, Y. P. Wang, Y. B. Chen, and S. L. Wang, *J. Solid State Chem.* **86,** 143 (1990) and references therein.
18. K. H. Lii, C. H. Li, T. M. Chen, and S. L. Wang, *Z. Kristallogr.* **197,** 67 (1991); V. Soghomonian, R. C. Haushalter, and J. Zubieta, submitted for publication.
19. K. H. Lii and C. S. Lee, *Inorg. Chem.* **29,** 3298 (1990).
20. S. L. Wang, H. Y. Kang, C. Y. Cheng, and K. H. Lii, *Inorg. Chem.* **30,** 3496 (1991).
21. K. H. Lii, and H. J. Tsai, *Inorg. Chem.* **30,** 446 (1991).
22. K. H. Lii and H. J. Tsai, *J. Solid State Chem.* **91,** 331 (1991).
23. A. V. Lavrov, V. P. Nikolaev, G. G. Sadikov, and M. A. Porai-Koshits, *Sov. Phys.—Sokl.(Engl. Transl.)* **27,** 680 (1982).
24. K. H. Lii, N. S. Wen, C. C. Su, and B. R. Chen, *Inorg. Chem.* **31,** 439 (1992).
25. A. V. Lavrov, V. P. Nikolaev, G. G. Sadikov, and M. Ya. Voitenkov, *Sov. Phys.—Vokl. (Engl. Transl.)* **26,** 631 (1981).
26. B. Klinert and M. Z. Jansen, *Z. Anorg. Allg. Chem.* **567,** 87 (1988).
27. C. Delmas, R. Olazcuaga, F. Cherkaoui, R. Brochu, and G. LeFlem, *C. R. Seances Acad. Sci., Ser. C* **287,** 169 (1978).
28. R. C. Haushalter, Z. Wang, M. E. Thompson, and J. Zubieta, submitted for publication; R. C. Haushalter, Z. Wang, M. E. Thompson, and J. Zubieta, *Inorg. Chem.*, in press.
29. R. C. Haushalter, Z. Wang, M. E. Thompson, and J. Zubieta, *Inorg. Chem.*, in press.
30. Q. Chen and J. Zubieta, *Inorg. Chem.* **29,** 1456 (1990); V. W. Day, and W. G. Klemperer, *J. Am. Chem. Soc.* **109,** 2991 (1987).

31. C. J. O'Connor, *Prog. Inorg. Chem.* **29,** 203 (1982).
32. H. T. Evans, *Inorg. Chem.* **30,** 501 (1984).
33. M. V. Capparelli, D. M. L. Goodgame, P. B. Hayman and A. C. Skapski, *J. Chem. Soc., Chem. Commun.*, 776 (1986).
34. V. W. Day, W. G. Klemperer, and D. J. Maltbie, *J. Am. Chem. Soc.* **109,** 2991 (1987).
35. I. D. Brown and D. Altermatt, *Acta Crystallogr., Sect. B* **41,** 244.
36. M. D. Robin and P. Day, *Adv. Inorg. Chem. Radiochem.* **10,** 247 (1967).
37. J. C. Bonner and M. E. Fisher, *Phys. Rev. A* **135,** 640 (1964).